Preparation and Quencher Diffusion Study of Pyrene-Tagged Water-Dispersible ABC Triblock Nanospheres

Gabriel Njikang,† Guojun Liu,*,† and Jun Gao‡

Department of Chemistry, Queen's University, 90 Bader Lane, Kingston, Ontario, Canada K7L 3N6, and Department of Physics, Queen's University, Kingston, Ontario, Canada K7L 3N6

Received June 7, 2007; Revised Manuscript Received September 12, 2007

ABSTRACT: A poly(glyceryl methacrylate)-*block*-poly[(2-hydroxyethyl methacrylate)-*ran*-(2-cinnamoyloxyethyl methacrylate)]-*block*-poly[(*tert*-butyl acrylate)-*ran*-(acrylic acid)-*ran*-(pyrenemethyl acrylamide)] or PGMA−P(HEMA−CEMA)−P(tBA−AA−Py) sample and a PGAM−PCEMA−P(tBA−AA−Py) sample were synthesized. Spherical micelles were prepared from the triblocks in water with a soluble PGMA corona, an insoluble P(HEMA−CEMA) or PCEMA shell, and an insoluble P(tBA−AA−Py) core. Photocrosslinking the P(HEMA−CEMA) or PCEMA layer yielded nanospheres. Driving I^- into the P(tBA−AA−Py) core led to pyrene fluorescence quenching. The decrease in pyrene fluorescence intensity as a function of time after quencher addition was used to examine how the rate of I^- diffusion changed with variations in the degree of CEMA crosslinking, in the degree of tBA hydrolysis in the core, and with addition of the plasticizer tetrahydrofuran into water.

I. Introduction

With the PGMA block water soluble, the P(HEMA−CEMA) block photocrosslinkable and permeable to a wide range of reagents, and the PtBA block readily hydrolyzable, poly(glyceryl methacrylate)-*block*-poly[(2-hydroxyethyl methacrylate)-*ran*-(2-cinnamoyloxyethyl methacrylate)]-*block*-poly(*tert*-butyl acrylate) or PGMA−P(HEMA−CEMA)−PtBA is a very useful polymer. We have, for example, prepared cylindrical micelles from such a triblock in water with PGMA as the corona, P(HEMA−CEMA) as the shell, and PtBA as the core.[1] Photocrosslinking of the P(HEMA−CEMA) shell led to structurally stable nanofibers, and further hydrolysis of the PtBA block yielded water-dispersible nanotubes with poly(acrylic acid) or PAA-lined cores. Such nanotubes were subsequently used as a host or template for the production of catalytic Pd particles[2] or superparamagnetic γ-Fe_2O_3[3] or Ni particles.[4] One can imagine similar applications for spherical micelles prepared in water from PGMA−P(HEMA−CEMA)−PtBA. Regardless of the end application of the PGMA−P(HEMA−CEMA)−PtBA nanospheres or nanofibers, the permeability of the crosslinked P(HEMA−CEMA) layer to external reagents, such as trifluoroacetic acid that catalyzes the hydrolysis of PtBA and Pd^{2+}, Fe^{2+}, and Ni^{2+} that are precursors to inorganic nanoparticles, is of critical importance. We report in this paper on how variations in structural parameters of the PGMA−P(HEMA−CEMA)−PtBA nanospheres, e.g., the degree of P(HEMA−CEMA) crosslinking and the degree of PHEMA cinnamation in the P(HEMA−CEMA) block, affect diffusion of I^- across the P(HEMA−CEMA) layer and in the nanosphere core.

This was done by first hydrolyzing a small fraction of the tBA units of the PtBA block into acrylic acid (AA) units and reacting the resultant AA units with pyrenemethyl amine to yield PGMA−P(HEMA−CEMA)−P(tBA−AA−Py) (structure is shown in Chart 1), where P(tBA−AA−Py) denotes poly[(*tert*-butyl acrylate)-*ran*-(acrylic acid)-*ran*-(pyrenemethyl acrylamide)]. The pyrene-tagged triblock was then used to prepare spherical micelles and nanospheres in water with an ideally layered structure as illustrated in Scheme 1. The diffusion of quencher KI across the P(HEMA−CEMA) layer and in the nanosphere core was followed from a pyrene fluorescence intensity decrease as a function of time after quencher addition.

For potential application of block copolymer micelles in controlled delivery,[5] release kinetics of drugs or drug model compounds from the core of diblock copolymer micelles[6−12] and vesicles[13,14] have been studied in the past. The diffusion process examined here is the opposite of the drug release process and may be viewed as an analogue of the drug loading process,[14,15] which has been less studied. This work differs from prior research for the fact that past studies have been mainly concerned with diblock copolymer micelles rather than ABC triblock copolymer micelles. Furthermore, past studies were concerned with uncrosslinked micelles or vesicles rather than crosslinked micelles or nanospheres. This study differs from prior studies also by the fact that we could compare the diffusion behavior of I^- in both the solid PGMA−P(HEMA−CEMA)−P(tBA−AA−Py) nanospheres and the hollow PGMA−P(HEMA−CEMA)−P(AA−Py) nanospheres with the latter bearing structural resemblance to ABC triblock copolymer vesicles.[16−18]

II. Experimental Section

Materials and Reagents. Hexane, methanol, and methylene chloride were of reagent grade from Fisher Scientific and were used without further purification. Stabilizer-free tetrahydrofuran (THF, 99.9%) from Fisher Scientific was purified by filtration through an Innovative Technology system. Pyridine (ACS reagent, Fisher Scientific) was refluxed and distilled over CaH_2 under nitrogen. Anhydrous *N*,*N*′-dimethylformamide (99.8%, DMF), 1-pyrenemethylamine hydrochloride (95%), 1-hydroxybenzotriazole (95%, HBT), *N*-(3-dimethylaminopropyl)-*N*-ethylcarbodiimide hydrochloride (commercial grade, EDCI), potassium iodide (99%), trifluoroacetic acid (TFA, 99%), cinnamoyl chloride (98%), and triethylsilane (99%) were purchased from Aldrich and were used as received. Phosphate buffer at pH = 7.0 and a potassium phosphate monobasic concentration of 0.050 M were purchased from Fisher Scientific. PGMA−P(HEMA−CEMA)−PtBA and PGMA−PCEMA−PtBA were prepared following literature procedures.[1,4]

PGMA−P(HEMA−CEMA)−P(tBA−AA−Py). PGMA−P(HEMA−CEMA)−PtBA, 50 mg, was dispersed in 2.4 mL of CH_2Cl_2.

* To whom correspondence should be addressed.
† Department of Chemistry.
‡ Department of Physics.

10.1021/ma071268e CCC: $37.00
Published on Web 11/15/2007

Chart 1

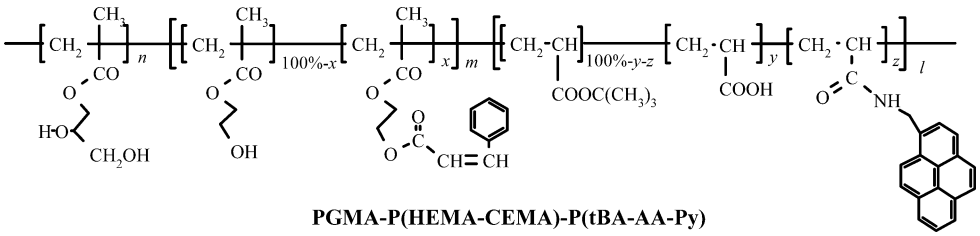

PGMA-P(HEMA-CEMA)-P(tBA-AA-Py)

Scheme 1. Cross-Sectional View of the Ideal Structure of a PGMA−P(HEMA−CEMA)−P(tBA−AA−Py) Nanosphere in Water, the Yellow Stars in the Core Denote Fluorescent Pyrene Groups

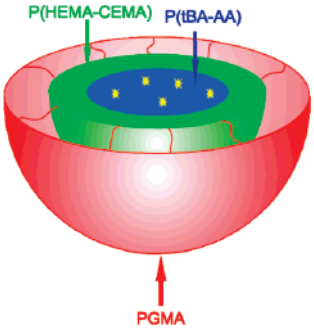

To the dispersion was then added 22 μL of triethylsilane and 125 μL of trifluoroacetic acid. The dispersion was stirred for 5 min before 0.5 mL MeOH was added, and the resultant mixture was added into excess hexane to precipitate the polymer. The precipitate was washed thrice by hexane before drying in a vacuum oven. NMR analysis indicated that ~2 mol % of the tBA groups were hydrolyzed to AA groups.

Pyrenemethylamine hydrochloride or $PyNH_2$·HCl was reacted with the AA groups via amidization catalyzed by EDCI. In an example run, 30 mg of PGMA−PCEMA−P(tBA−AA) and 5.4 mg of $PyNH_2$·HCl were dissolved in 1.0 mL of DMF in a 50 mL round-bottom flask. To it was added a mixture consisting of 0.2 mL of DMF, 7.7 mg of EDCI, 4.1 mg of *N*-hydroxysuccinamide, 60 μL of 0.050 M phosphate buffer at pH 7.0, and 80 μL of H_2O. The resultant solution was stirred at room temperature overnight before it was dialyzed in a tube with molecular weight cut-off (MWCO) = 12 000−14 000 against methanol changed 5 times over 3 days. The mixture was then concentrated by rota-evaporation to ~0.5 mL, precipitated in 3.5 mL of ether, and dried in a vacuum oven.

PGMA−P(HEMA−CEMA)−P(tBA−AA−Py) Spheres. PGMA−P(HEMA−CEMA)−P(tBA−AA−Py), 30 mg, was dissolved in 2 mL of pyridine. Under vigorous stirring, to it was added 2 mL of water at ~0.033 drop/s using a syringe having a PrecisionGlide 20G11/2 needle. This was followed by the addition of another 63 mL of water in one aliquot. The resultant solution was heated at 50 °C overnight before it was dialyzed in a tube with MWCO = 12 000−14 000 against H_2O changed 20 times over 48 h. Nanospheres were obtained by irradiating the micellar solution with a focused beam from a 500 W Hg lamp that had passed through a bandpass filter centered at 298 nm with a peak transmission of 70% and a half width of 2.5 nm at half transmission height until a desired PCEMA double bond conversion β was reached as determined by UV absorbance measurements at 274 nm. The nanospheres were then dialyzed in a tube with MWCO = 500 000 first against methanol to remove small-molecule pyrene. Once the amount of pyrene in the dialysate became negligible as determined by steady-state fluorescence analysis, the solution was dialyzed against water for solvent exchange. Nanospheres were stored in this solvated state under constant stirring until analysis. Hollow-spheres were produced through hydrolysis of the remaining tBA units to AA following procedures reported for the production of PGMA−PCEMA−PAA nanotubes.[1,4]

Techniques. Size exclusion chromatography (SEC) was performed on a Waters 515 system equipped with three columns (one μStyragel 500 Å and two styragel HR 5E columns) and a differential refractometer (Water 2410), both equilibrated at 36 °C. The system was calibrated by monodisperse polystyrene standards. The eluant used was DMF containing 0.25% tetrabutylammonium bromide at a flow rate of 0.4 mL/min. Proton nuclear magnetic resonance (^{1}H NMR) spectra were recorded on a Bruker Advance 300 MHz spectrometer with either deuterated chloroform or pyridine as the solvent. Light scattering measurements were carried out on a Brookhaven BI-200 SM instrument equipped with a BI-9000AT digital correlator and a He−Ne laser (632.8 nm) at 22 °C. Dynamic light scattering (DLS) measurements were done at 90°, and samples were clarified by filtration through 0.45 μm Titan2 regenerated cellulose filters. The data were treated by the cumulant method[19] to yield particle hydrodynamic diameter d_h and polydispersity K_2^2/K_4.

Tapping mode atomic force microscopy (AFM) studies were performed on a Veeco multimode microscope equipped with a Nanoscope IIIa controller using silicon tips with a force constant and oscillating frequency at approximately 40 N/m and approximately 300 kHz, respectively. Specimens for AFM were prepared by aspirating sample solutions onto freshly cleaved mica. Transmission electron microscopy (TEM) measurements were carried out on a Hitachi H-7000 instrument operated at 75 kV. The specimens for TEM were prepared by aspirating the sample solutions on carbon coated or nitro cellulose copper grids. The TEM specimens were stained with OsO_4 vapor for 2 h or uranyl acetate in methanol/H_2O (1:9 v/v) at a concentration of 0.05 g/mL for 30 min before observations. Excess uranyl acetate was removed by dropping water on the specimen using a Pasteur pipet and sucking it off with filter paper. This cleaning process was repeated 10 times

Fluorescence Experiments. All steady-state fluorescence measurements were done in deionized water in Hellma quartz cells using a Photon Technology International Alphascan spectrophotometer with a 150 W xenon compact light source. For the Stern−Volmer plots, the $PyNH_2$·HCl solution concentration used was 4.0 μM. Quencher solutions at 0.130 M were added in 10.0 μL aliquots into 3.00 mL of $PyNH_2$·HCl solution. After the addition of each quencher aliquot, the mixture was swirled rapidly on a Vortex instrument for 30 s and equilibrated for 1 h before fluorescence measurements. The excitation wavelength used was 342 nm, and the excitation and emission slit widths used were 3.0 and 0.5 nm, respectively.

A typical quencher diffusion kinetic experiment involved adding 150 μL of a 8.4 M KI solution into 2.60 mL of a nanosphere solution at ~0.14 mg/mL in either water or water/THF (at 99:1 v/v). The mixture was then shaken vigorously and quickly transferred to the spectrophotometer for time-dependent fluorescence measurement. The excitation and emission wavelengths used were 342 and 396 nm. To minimize photobleaching, the excitation and emission slit widths used were 1.0 and 10 nm, respectively. To examine the effect of quencher concentration variation, the above experimental protocol was maintained except the concentration of the KI stock solution used was changed from 8.4 to 8.0, 6.0, 4.0, and 2.0 M, respectively.

III. Results and Discussion

Triblock Preparation and Characterization. A PGMA−PCEMA−P(tBA−AA−Py) sample, P1, and a PGMA−P(HE-

Table 1. Characteristics of the PSMA−PCEMA−PtBA Sample

dn_r/dc (mL/g)	LS M_w (g/mol)	SEC M_w/M_n	NMR $n/m/l$	n	M	l
0.117	2.1×10^5	1.35	1:0.21:0.25	760	160	190

MA−CEMA)−P(tBA−AA−Py) sample, P2, were used in this study. To synthesize P1 and P2, we first reacted PSMA−PHEMA−PtBA with an excess and a controlled amount of cinnamoyl chloride to yield PSMA−PCEMA−PtBA and PSMA−P(HEMA−CEMA)−PtBA.[1,20] The polymers were then stirred in THF containing 6.0 M hydrochloric acid to hydrolyze PSMA to yield PGMA−PCEMA−PtBA and PGMA−P(HEMA−CEMA)−PtBA. Further treating the polymers in CH_2Cl_2 containing 5 vol % of TFA for 5 min hydrolyzed ~2 mol % tBA units to yield PGMA−PCEMA−P(tBA−AA) and PGMA−P(HEMA−CEMA)−P(tBA−AA). The polymers were subsequently reacted with $PyNH_2$·HCl in DMF containing aqueous pH 7.0 buffer to attach pyrene to a fraction of the AA units to yield P1 and P2. Addition of an aqueous phosphate buffer to DMF in amidization was of critical importance because EDCI could also catalyze esterification between the hydroxyl groups and carboxyl groups of PGMA−PCEMA−P(tBA−AA) or PGMA−P(HEMA−CEMA)−P(tBA−AA) in the absence of water. The selective amidization under our experimental conditions in the presence of water is well documented for proteins and enzymes and was experimentally verified for our systems by the observation that both the molar masses or molar mass distributions of P1 and P2 remained essentially identical to those of their precursory PGMA−PCEMA−P(tBA−AA) and PGMA−P(HEMA−CEMA)−P(tBA−AA). We removed the unreacted $PyNH_2$·HCl by prolonged dialysis and the amount of pyrene groups attached was estimated from UV−visible absorbance analyses to be 2.56 mg/g polymer and 2.16 mg/g polymer for P1 and P2 with the degrees of cinnamation of 100% and 85%, respectively.

We fully characterized PSMA−PCEMA−PtBA to yield the n, m, and l numbers for P1 and P2 (see Table 1). The triblock was characterized in the PSMA−PCEMA−P*t*BA form for the analogous solubility of PSMA, PCEMA, and PtBA. All three blocks of PSMA−PCEMA−PtBA dissolve, for example, in butanone, tetrahydrofuran (THF), chloroform, and *N*,*N*-dimethylforamide (DMF), etc. In contrast, PGMA dissolves only in polar solvents such as water and methanol in which PCEMA is insoluble. The specific refractive index increment dn_r/dc and light scattering (LS) weight-average molar mass M_w were determined in butanone because it had the lowest refractive index among butanone, THF, chloroform, and DMF, and its use afforded a sufficiently large dn_r/dc value to reduce measurement errors in dn_r/dc and M_w. The size exclusion chromatography (SEC) polydispersity index M_w/M_n was determined in DMF based on polystyrene standards, and the number of repeat unit ratios $n/m/l$ were determined from comparing intensities of characteristic peaks of the three blocks from ^{1}H NMR spectra measured in $CDCl_3$. Combining the LS M_w and NMR $n/m/l$ we obtained the weight-average number of repeat units of 760, 160, and 190 for PSMA, PCEMA, and PtBA, respectively.

Nanospheres. Nanosphere preparation from P1 and P2 first invoked micelle formation in pyridine/water with 97 vol % of water. The micellar samples were annealed at 50 °C overnight before the pyridine was removed by dialysis against deionized water at room temperature. Nanospheres were obtained after CEMA crosslinking under UV irradiation. To minimize photodamaging of pyrene, the irradiation was done with light that passed through a bandpass filter centered at 298 nm where pyrene absorbed relatively weakly and CEMA absorbed strongly.

Three types of nanospheres were prepared from P1 and P2. Nanosphere type 1 or N1 was prepared from P1. With dependence on the CEMA double bond conversion β, N1 spheres were divided further into N1-24% and N1-32% spheres, where the numbers after the hyphens denoted the β values. Nanosphere type 2 or N2 was prepared from P2. The β value in this case was also 32%. Type 3 nanospheres were derived from N1-32% nanospheres after the quantitative hydrolysis of the core tBA groups following a method used extensively in our research group.[21−23]

Figure 1 shows a TEM and an AFM image for N1-32% nanospheres. The TEM image shows that most of the particles have a light core and a dark shell or a core−shell structure. Averaging over all of the core−shell particles in the TEM image in Figure 1, we obtained a core−shell diameter d_{TEM} of 30 ± 3 nm and a shell thickness of 7 ± 5 nm. We further determined an AFM diameter d_{AFM} of 59 ± 4 nm for the nanospheres. The fact that d_{AFM} was substantially larger than d_{TEM} and only the PCEMA layer should be stained by OsO_4 and appear dark in a TEM image suggests that the nanospheres possessed a P(tBA−AA−Py) core, a PCEMA shell, and a PGMA corona that was not visible by TEM but by AFM. The core−shell−corona structure assignment is reasonable because only PGMA is water soluble, PCEMA and PtBA are immisicible,[24,25] and the aggregation of the terminal PtBA block into the core rather than the shell is favored entropically. Furthermore, one should also realize that we have previously prepared cylindrical micelles in water from a similar PGMA−PCEMA−PtBA triblock and the core−shell−corona assignment was established unambiguously there by our ability to process the micelles to yield nanotubes and then load Pd or Ni into the cores of the nanotubes.[4]

We further determined a hydrodynamic diameter d_h value of 89 ± 1 nm from DLS for this sample. This value was larger than d_{AFM} because AFM and DLS probed the size of the nanospheres in their dry and solvated states, respectively.

We also obtained d_{TEM}, d_{AFM}, and d_h as well as DLS polydispersities K_2^2/K_4 for the other samples with results shown in Table 2. Data in the table show that neither the size nor the size distribution changed significantly among the different particles. This size and size distribution invariance with β is in agreement with our prior observation that PCEMA photocrosslinking did not perturb but only locked in the structure of the block copolymer micelles.[26]

We see in the TEM image also some smaller particles, as marked by arrows. These particles do not possess the core−shell structure but only a dark core. The presence of such smaller particles, although small in number, is seen also in the AFM images. We suspect that these particles were derived from the contaminating diblock PGMA−PCEMA, which should be present as judged from the high polydispersity index of 1.35 for PSMA−PCEMA−PtBA. We did not exhaust our means to separate the diblock contaminant because we suspected that these particles did not contain the P(tBA−AA−Py) block and should thus not contribute to the fluorescence data. Furthermore, this study has been only exploratory and is semiquantitative in nature.

While PtBA and PCEMA should segregate, the block segregation should definitely not be as sharp as what is depicted in Scheme 1. As mentioned before, we estimated from the TEM image of Figure 1 a core diameter of 16 nm. On the basis of this number, the model of Scheme 1, and the mass ratio of 1.7 between PCEMA and PtBA, we calculated a shell thickness of 3.2 nm by assuming densities of ~1 g/mL for the two polymers.

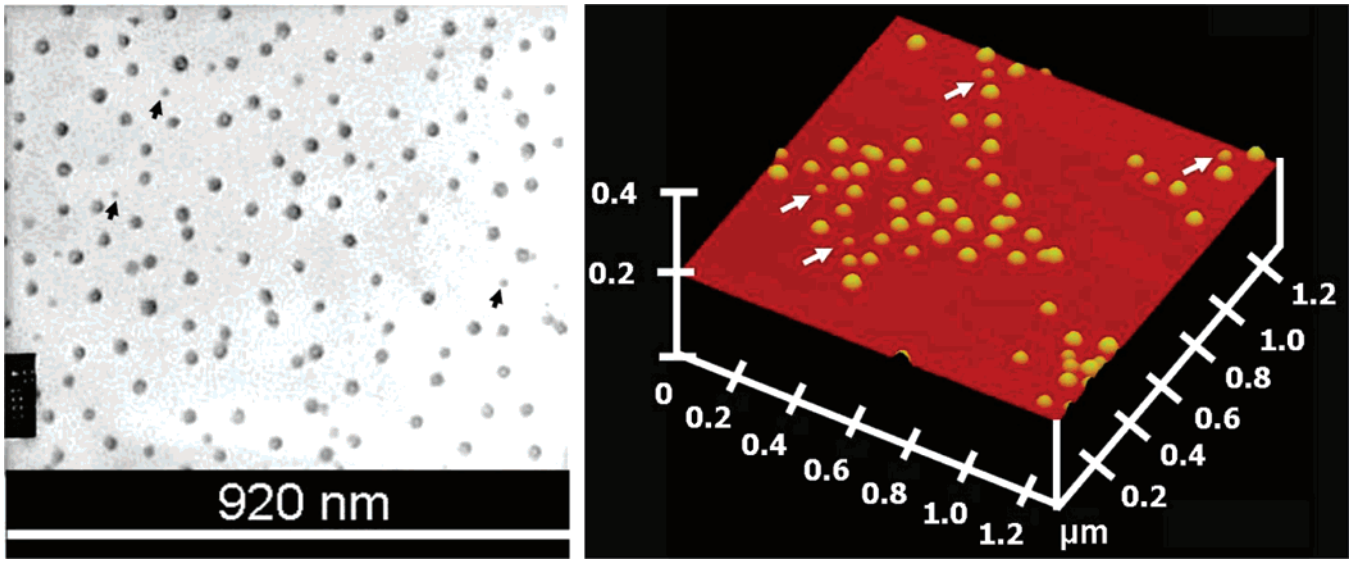

Figure 1. TEM (left) and AFM (right) images of nanosphere N1-32%.

Table 2. Characteristics of PGMA−P(HEMA−CEMA)−P(tBA−AA−Py) Micelles and Nanospheres

CEMA double bond conversion β	d_h (nm)	K_2^2/K_4	d_{TEM} (nm)	d_{AFM} (nm)
P1 Micelles or Nanosphere Type 1				
0	89 ± 1	0.05 ± 0.03	29 ± 2	58 ± 4
24%	89 ± 1	0.04 ± 0.03	31 ± 3	59 ± 6
32%	89 ± 1	0.04 ± 0.02	30 ± 3	59 ± 4
P2 Micelles or Nanosphere Type 2				
0%	88 ± 1	0.04 ± 0.03	30 ± 3	57 ± 6
32%	88 ± 1	0.06 ± 0.04	31 ± 4	56 ± 3
Nanosphere Type 3				
32%	91 ± 1	0.05 ± 0.03	30 ± 3	60 ± 5

The significant difference between 3.2 nm and 7 ± 5 nm can be partially attributed to errors in the determined value of 7 ± 5 nm. This was caused more likely by the incomplete phase separation between PCEMA and PtBA and thus a diffuse stained PCEMA layer at the PCEMA and PtBA interface. For PS and poly(methyl methacrylate), the interface thickness was found experimentally to be 4.9 nm[27] and a comparable value is expected for the interface between PCEMA and PtBA.

Pyrene Emission. Figure 2 compares the fluorescence emission spectra of $PyNH_2$·HCl, nanosphere N1-32%, and hollow nanosphere N3-32% in water. The intensity of excimer emission[28] between 440 and 600 nm is low for every sample, confirming the low pyrene content in the nanosphere cores. Compared with $PyNH_2$·HCl emission, the peaks of the nanospheres are red-shifted by 1.5 nm and the peak positions of the N1-32% and N3-32% spheres coincide with each another. Since the pyrene groups were surrounded by mostly tBA groups in the N1 nanospheres and by AA groups in the N3 spheres, the insignificant peak position differences in these two cases suggest the low solvachromic effect of the pyrene chromophore, a result in agreement with previous observations.[29]

Pyrene has typically five prominent emission peaks between ~370 and ~400 nm.[30] The relative emission intensity between the first and third vibronic peaks, I_1/I_3, has been traditionally used to provide a measure for the local polarity of pyrene.[29] For $PyNH_2$·HCl, its second vibronic band is not obvious and the first and third peaks occur at 374.5 and 384.5 nm, respectively, with $I_1/I_3 = 2.68$. I_1/I_3 changed to 1.61 for N3-32% and 1.42 for N1-32% spheres, suggesting the increasing polarity when the core was changed from P(tBA−AA−Py) to P(AA−Py).

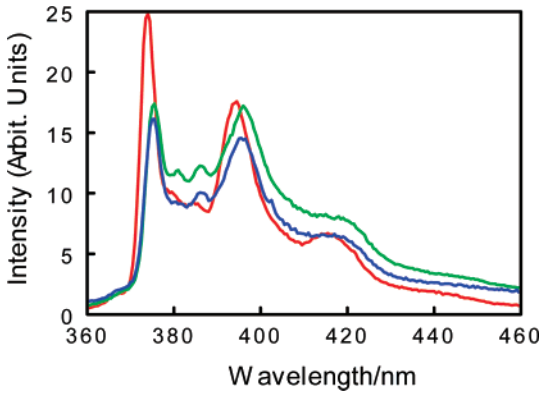

Figure 2. Comparison of fluorescence spectra of $PyNH_2$·HCl (red), hollow nanosphere N3-32% (blue), and nanosphere N1-32% (green).

Selection of $PyNH_2$·HCl Fluorescence Quencher. I^- and Tl^+ are known to undergo collisional quenching of fluorescence of many chromophores due to the heavy atom effect,[31] and they quenched $PyNH_2$·HCl fluorescence as expected. Analysis of the dependence of $PyNH_2$·HCl fluorescence intensity in deionized water as a function of concentration using the Stern−Volmer equation for the two quenchers yielded the $k_q\tau_0$ values of 2.8 × 10^2 and 7.8 × 10^2 M^{-1} for Tl^+ and I^-, respectively. Since the lifetime τ_0 of $PyNH_2$·HCl in air-saturated water should be ~100 ns,[32] the quenching rate constants k_q for Tl^+ and I^- are thus ~2.8 × 10^9 and ~7.8 × 10^9 M^{-1} s^{-1} with the latter approaching the diffusion-controlled quenching constant of pyrene fluorescence by I^-.[33,34] Because of the lower quenching efficiency of Tl^+ and also for the much lower solubility of $TlNO_3$ than KI in water, we did not use $TlNO_3$ but only KI as a quencher for the nanospheres.

Acquisition and Treatment of Quencher Diffusion Kinetic Data. As mentioned in the Introduction, the main objective of this study was to establish a method probing kinetics of reagent diffusion across the P(HEMA−CEMA) layer and in the nanosphere core. Using the targeted nanospheres with structure shown in Scheme 1, we could probe quencher diffusion via a simple experiment as described in the Experimental Section.

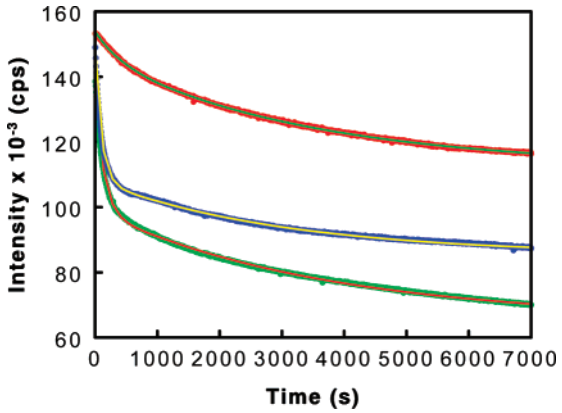

Figure 3. Data of pyrene fluorescence intensity decrease as a function of time after KI addition to N1-32% (red data points and green fit) and N2-32% (blue data points and yellow fit) nanospheres in water and N1-32% in water containing 1 vol % of THF (green data and red fit).

Such an experiment involved addition of I^- into a nanosphere solution at time $t = 0$ and then the monitoring of pyrene fluorescence intensity decrease with time. Figure 3 shows three sets of such data.

While getting data of the type shown in Figure 3 was trivial, getting data that genuinely belonged to the nanospheres required attention to details. For example, in the early stage of this project we noticed ~2 s after I^- addition, a pyrene fluorescence intensity decrease that was 3−4 times more than what could be accounted for by the dilution effect. This suggested the presence of small-molecule pyrene in the aqueous phase and prompted us to clean the samples more by subjecting the nanosphere solutions to further dialysis against methanol in a tube with MWCO = 500 000. The further treatment helped eliminate the unwarranted instantaneous intensity drop almost completely and thus removed small-molecule pyrene species.

We also debated if O_2 should be removed in the florescence quenching experiments and decided not to remove O_2 for the following reasons. First, we reasoned that the presence of O_2 might change the fluorescence quenching efficiency result somewhat for a given sample but should have a minimal effect on the quencher diffusion result, which was the key information that we sought. Second, we are more interested in diffusion rate variation trends rather than the absolute diffusion coefficients because of the difficulty to treat the quenching data quantitatively as will be discussed later. The consistent presence of O_2 in every one of a series of samples should not change the variation trends in neither the diffusion rates nor the quenching efficiencies. Third, results from this study were to be used to help understand the process of loading into nanospheres of potentially useful reagents such as Ni^{2+}, Pd^{2+}, and drugs. The loading of these reagents is normally done under ambient conditions and not in the absence of O_2, and the fluorescence quenching experiments should thus be performed to reflect these experimental conditions.

Data such as those in Figure 3 can in principle be treated with rigor. For example, one can assume the validity of classical diffusion equations in such core−shell composite spheres and solve for quencher concentration profiles $c_q(r,t)$ at different times t and distances r from the particle center.[35,36] Assuming a reasonable relation between $c_q(r,t)$ and the efficiency of fluorescence quenching, one can further obtain theoretical expressions for pyrene fluorescence intensity $F(t)$ change as a function of time. This task is, however, more easily stated than

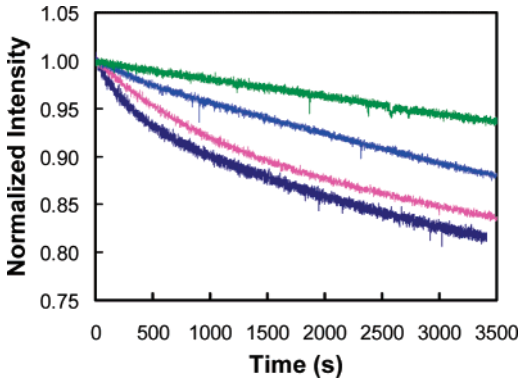

Figure 4. Comparison of N1-32% fluorescence intensity decrease data as a function of time after KI addition at 0.11 (top), 0.22 (second from top), 0.33 (third from top), and 0.44 M (bottom), respectively.

achieved because the mathematical solution for diffusion equations in such core−shell spheres or more precisely core−shell spheres with a diffuse boundary layer of an unknown thickness and varying diffusion coefficients in different regions of the particle is a very formidable task.[35]

For the above reason, we have treated the experimental data only by the following phenomenological expression:

$$F(t) = F_\infty + F_1 \, e^{-k_1 t} + F_2 \, e^{-k_2 t} \tag{1}$$

where F_∞ is the residual fluorescence intensity at time $t \rightarrow \infty$ under a given set of experimental conditions and F_1 and F_2 are fluorescence intensities quenched with rate constants k_1 and k_2, respectively. Thus, the ultimate efficiency of pyrene fluorescence quenching at a given bulk quencher concentration is

$$\phi = \frac{F_1 + F_2}{F_\infty + F_1 + F_2} \tag{2}$$

and the average rate constant for quencher diffusion is

$$\langle k \rangle = \frac{k_1 F_1 + k_2 F_2}{F_1 + F_2} \tag{3}$$

Physical Significance of Equation 1. We chose eq 1 to treat the experimental data purely out of convenience. Despite the arbitrariness on our part, such an equation has been used in treating fluorescence quenching data of carboxyfluorescein[37] and CdS[38] encapsulated in the core of lipid vesicles by protons and benzyl alcohol diffusing through the membrane layer. In such cases, the k_1 and k_2 values were assigned physical meanings and used to calculate permeability constants of quenchers across the vesicle membranes.

If k_1 and k_2 are real rate constants in our case, they should be quencher concentration independent. Figure 4 compares N1-32% fluorescence intensity decrease data as a function of time after KI addition at final concentrations of 0.11, 0.22, 0.33, and 0.44 M, respectively. The data show clearly that the extent of fluorescence quenching at a given time increased expectantly as the quencher concentration increased.

Unfortunately, the shape of the quenching kinetic curves changed with KI concentration as well. This thus suggests that the k_1 and k_2 values are not concentration independent and are not directly related to intrinsic properties of the system such as the diffusion coefficients of the I^- and the radius of the nanospheres.

While the meanings of k_1 and k_2 are ambiguous, it is easy to understand why a significant fraction of fluorescence $1 - \phi$ may not be quenched for the N1 and N2 spheres even at

Table 3. Quencher Diffusion Kinetic Results Obtained from Pyrene Fluorescence Quenching Experiments, the Final KI Concentration Was Always 0.46 M

sample	solvent	$k_1 \times 10^3$ (s^{-1})	$k_2 \times 10^4$ (s^{-1})	ϕ (%)	$\langle k \rangle \times 10^4$ (s^{-1})
N1-32%	H_2O	2.53	2.94	27.1	7.1
N1-32%	H_2O	1.50	2.90	28.5	5.2
average		2.01 ± 0.51	2.92 ± 0.02	(27.8 ± 0.7)	6.1 ± 1.0
N1-24%	H_2O	2.17	1.74	39	9.5
N1-24%	H_2O	2.75	2.53	39	12.2
average		2.46 ± 0.19	2.13 ± 0.40	(39 ± 1)	10.8 ± 1.4
N1-32%	H_2O/THF	7.8	2.73	53	44
N1-32%	H_2O/THF	7.4	3.3	53	46
average		7.6 ± 0.2	3.0 ± 0.3	(53 ± 1)	45 ± 1
N2-32%	H_2O	5.5	2.65	47	32
N2-32%	H_2O	10.0	3.3	43	65
average		7.7 ± 2.3	3.0 ± 0.3	(45 ± 2)	49 ± 17
N3-32%	H_2O	16.5	34	97	115
N3-32%	H_2O	14.4	34	97	93
average		15.5 ± 1.0	34 ± 1	(97 ± 1)	104 ± 11

infinitely long times at a given bulk quencher concentration. First, a certain portion of the nanosphere cores may be simply inaccessible. Second, the concentration of the quencher in the accessible part of the nanosphere P(tBA−AA−Py) cores may be much lower than that in the solvent phase for unfavorable I^- partition. In the cores of such spheres with low I^- diffusivity, we suspect that the pyrene fluorescence is quenched by I^- only if pyrene is within distances defined by a quenching sphere of volume υ.[39] The Stern−Volmer equation under such circumstances is then

$$F(0)/F_\infty = \exp\left(\frac{[Q]_c \upsilon N_A}{1000}\right) \quad (4)$$

with $F(0)$ being pyrene fluorescence intensity at time zero, N_A being Avogadro's number, and $[Q]_c$ being the equilibrium I^- concentration in the accessible part of the core. Equation 4 shows clearly that $F(0)/F_\infty$ takes finite values if $[Q]_c$ is small.

Diffusion Kinetic Results. Despite ambiguity in the physical meanings of k_1 and k_2, they should be useful for viewing quencher diffusion rate variation trends when they are measured at a given quencher concentration for different samples. Shown in Table 3 are quencher diffusion kinetic results obtained for different nanosphere samples from data treatment using eq 1.

Results of Table 3 reveal the following features. First, ϕ can be determined with high precision and the error is typically below ±5% . Second, the experimental error for k_1, k_2, and $\langle k \rangle$ and in particular for k_1 is unfortunately significantly larger with error margin up to ±30%. While errors in ϕ were most likely caused by our instrument's inability to correct for excitation light intensity fluctuation and drifting, the large error in k_1 was probably due to our inability to capture the fast diffusion event represented by k_1 in whole.

Factors Affecting I^- Diffusion. Despite the low precision in the k values, we can conclude with confidence the following: First, decreasing the degree of PCEMA crosslinking or the conversion β of PCEMA double bonds from 32% to 24% increased not only ϕ but also k. The k increase with decreasing β can be due to increased I^- diffusion coefficient D. The ϕ increase, according to eq 4, suggests that the equilibrium I^- concentration $[Q]_c$ inside the P(tBA−AA−Py) core may increase with decreasing β.

We note that the addition of only 1 vol % of THF into water increased both ϕ and k pronouncedly. This must have derived from the profound plasticization effect of THF inside both the PCEMA shell and in the P(tBA−AA−Py) core. The swelling of the nanosphere core and shell by THF should increase not only the rate of I^- diffusion but also its solubility in these regions. The increase in ϕ and k can be accomplished also by retaining some of the HEMA units in the P(HEMA−CEMA) block. This explains why we had trouble loading Ni^{2+} and Pd^{2+} into PGMA−PCEMA−PAA but not PGMA−P(HEMA−CEMA)−PAA nanotubes.[2,4]

Both the k and ϕ values increased drastically for the hollow PGMA−PCEMA−P(AA−Py) spheres relative to the solid PGMA−PCEMA−P(tBA−AA−Py) spheres. The ϕ value should increase because $[Q]_c$ should increase inside the water-swollen core of PAA, which was obtained by removing the *tert*-butyl groups or 44.5 wt % of the matter from PtBA, for the improved compatibility between PAA and I^- and for the new void space available. The hydrolysis of PtBA should also increase the diffusivity of I^- inside the core significantly and turn on the collisional quenching mechanism. The ϕ value did not go to 99+% because we did not subtract the background fluorescence or scattering from the nanospheres themselves, which have been shown to be weak but present for a PGMA−PCEMA−PtBA nanosphere sample.

IV. Conclusions

We have successfully prepared and characterized a PGMA−P(HEMA−CEMA)−P(tBA−AA−Py) and a PGMA−PCEMA−P(tBA−AA−Py) sample. Spherical micelles were prepared from the polymers in water and were then irradiated by UV light to crosslink the P(HEMA−CEMA) or PCEMA shell to yield nanospheres. Pyrene emission from the core of such nanospheres was essentially free of the excimer peak. Addition of KI led to a gradual decrease in the pyrene emission intensity due to diffusion of I^- into the nanosphere core. The quenching kinetic data were fitted by a double exponential function to yield diffusion rate constants k_1 and k_2, average rate constant $\langle k \rangle$, as well as ultimate efficiency ϕ of pyrene fluorescence quenching by I^-. A comparison of the $\langle k \rangle$ and ϕ values of different samples concludes that I^- diffusion was increased by decreasing the degree of CEMA crosslinking, decreasing CEMA content in the P(HEMA−CEMA) block, adding plasticizer THF for the P(HEMA−CEMA) shell and the P(tBA−AA−Py) core, and hydrolyzing the PtBA core. While these trends are expected intuitively, results of this study have enabled a semiquantification of these effects.

Acknowledgment. We thank NSERC for sponsoring this research. G.L. thanks the CRC Program for a Canada Research Chair position in materials science.

References and Notes

(1) Yan, X. H.; Liu, G. J.; Li, Z. *J. Am. Chem. Soc.* **2004**, *126*, 10059−10066.

(2) Li, Z.; Liu, G. J. *Langmuir* **2003**, *19*, 10480−10486.
(3) Yan, X. H.; Liu, G. J.; Liu, F. T.; Tang, B. Z.; Peng, H.; Pakhomov, A. B.; Wong, C. Y. *Angew. Chem., Int. Ed.* **2001**, *40*, 3593−3596.
(4) Yan, X. H.; Liu, G. J.; Haeussler, M.; Tang, B. Z. *Chem. Mater.* **2005**, *17*, 6053−6059.
(5) Kataoka, K.; Harada, A.; Nagasaki, Y. *Adv. Drug Delivery Rev.* **2001**, *47*, 113−131.
(6) Teng, Y.; Morrison, M. E.; Munk, P.; Webber, S. E.; Prochazka, K. *Macromolecules* **1998**, *31*, 3578−3587.
(7) Stepanek, M.; Krijtova, K.; Limpouchova, Z.; Prochazka, K.; Teng, Y.; Munk, P.; Webber, S. E. *Acta Polym.* **1998**, *49*, 103−107.
(8) Giacomelli, C.; Le Men, L.; Borsali, R.; Lai-Kee-Him, J.; Brisson, A.; Armes, S. P.; Lewis, A. L. *Biomacromolecules* **2006**, *7*, 817−828.
(9) Sant, V. P.; Smith, D.; Leroux, J. C. *J. Controlled Release* **2005**, *104*, 289−300.
(10) Liu, G. J.; Zhou, J. Y. *Macromolecules* **2003**, *36*, 5279−5284.
(11) Liu, G. J.; Zhou, J. Y. *Macromolecules* **2002**, *35*, 8167−8172.
(12) Zhou, J. Y.; Li, Z.; Liu, G. J. *Macromolecules* **2002**, *35*, 3690−3696.
(13) Ding, J. F.; Liu, G. J. *J. Phys. Chem. B* **1998**, *102*, 6107−6113.
(14) Choucair, A.; Soo, P. L.; Eisenberg, A. *Langmuir* **2005**, *21*, 9308−9313.
(15) Wu, J.; Eisenberg, A. *J. Am. Chem. Soc.* **2006**, *128*, 2880−2884.
(16) Liu, F. T.; Eisenberg, A. *J. Am. Chem. Soc.* **2003**, *125*, 15059−15064.
(17) Rodriguez-Hernandez, J.; Lecommandoux, S. *J. Am. Chem. Soc.* **2005**, *127*, 2026−2027.
(18) Zheng, R. H.; Liu, G. J. *Macromolecules* **2007**, *40*, 5116−5121.
(19) Berne, B. J.; Pecora, R. *Dynamic Light Scattering with Applications to Chemistry, Biology, and Physics*; Dover Publications, Inc.: Mineola, NY, 1976.
(20) Liu, F. T.; Liu, G. J. *Macromolecules* **2001**, *34*, 1302−1307.
(21) Lu, Z. H.; Liu, G. J.; Phillips, H.; Hill, J. M.; Chang, J.; Kydd, R. A. *Nano Lett.* **2001**, *1*, 683−687.
(22) Lu, Z. H.; Liu, G. J.; Liu, F. T. *Macromolecules* **2001**, *34*, 8814−8817.
(23) Lu, Z. H.; Liu, G. J.; Duncan, S. *Macromolecules* **2004**, *37*, 174−180.
(24) Liu, G. J.; Ding, J. F.; Guo, A.; Herfort, M.; Bazett-Jones, D. *Macromolecules* **1997**, *30*, 1851−1853.
(25) Liu, G. J.; Ding, J. F.; Hashimoto, T.; Kimishima, K.; Winnik, F. M.; Nigam, S. *Chem. Mater.* **1999**, *11*, 2233−2240.
(26) Tao, J.; Stewart, S.; Liu, G. J.; Yang, M. L. *Macromolecules* **1997**, *30*, 2738−2745.
(27) Rharbi, Y.; Winnik, M. A. *Macromolecules* **2001**, *34*, 5238−5248.
(28) Winnik, M. A. *Acc. Chem. Res.* **1985**, *18*, 73−79.
(29) Dong, D. C.; Winnik, M. A. *Can. J. Chem.* **1984**, *62*, 2560−2565.
(30) Kalyanasundaram, K.; Thomas, J. K. *J. Am. Chem. Soc.* **1977**, *99*, 2039−2044.
(31) Turro, N. J. *Modern Molecular Photochemistry*; Benjamin/Cummings Publishing Co.: Menlo Park, CA, 1978.
(32) Ribou, A. C.; Vigo, J.; Salmon, J. M. *Photochem. Photobiol.* **2004**, *80*, 274−280.
(33) Morrison, M. E.; Dorfman, R. C.; Clendening, W. D.; Kiserow, D. J.; Rossky, P. J.; Webber, S. E. *J. Phys. Chem.* **1994**, *98*, 5534−5540.
(34) Birks, J. B. *Photophysics of Aromatic Molecules*; Wiley-Interscience: London, U.K., 1970.
(35) Carslaw, H. S.; Jaeger, J. C. *Conduction of Heat in Solids*, 2nd ed.; Clarendon: Oxford, U.K., 1959.
(36) Crank, J. *The Mathematics of Diffusion*, 1st ed.; Clarendon Press: Oxford, U.K., 1956.
(37) Kuyper, C. L.; Kuo, J. S.; Mutch, S. A.; Chiu, D. T. *J. Am. Chem. Soc.* **2006**, *128*, 3233−3240.
(38) Horvath, O. *Langmuir* **1999**, *15*, 279−281.
(39) Lakowicz, J. R. *Principles of Fluorescence Spectroscopy*; Plenum: New York, 1983.

MA071268E